The influence of Citrate or PEG coating on silver nanoparticle toxicity to a human keratinocyte cell line

Title: The influence of Citrate or PEG coating on silver nanoparticle toxicity to a human keratinocyte cell line

Author: V. Bastos J.M.P. Ferreira de Oliveira D. Brown H. Jonhston E. Malheiro A.L. Daniel-da-Silva I.F. Duarte C. Santos H. Oliveira

PII: S0378-4274(16)30041-8
DOI: http://dx.doi.org/doi:10.1016/j.toxlet.2016.03.005
Reference: TOXLET 9337

To appear in: *Toxicology Letters*

Received date: 5-1-2016
Revised date: 3-3-2016
Accepted date: 21-3-2016

Please cite this article as: Bastos, V., Ferreira de Oliveira, J.M.P., Brown, D., Jonhston, H., Malheiro, E., Daniel-da-Silva, A.L., Duarte, I.F., Santos, C., Oliveira, H., The influence of Citrate or PEG coating on silver nanoparticle toxicity to a human keratinocyte cell line.Toxicology Letters http://dx.doi.org/10.1016/j.toxlet.2016.03.005

Highlights of the manuscript Bastos et al (TOXLET-D-16-00023) "The influence of Citrate or PEG coating on silver nanoparticle toxicity to a human keratinocyte cell line":

. PEG and citrate coatings strongly determine AgNPs toxicity

. AgNPs surface coating influences the mechanisms of cell death

. Citrate-coated AgNPs have more severe cytotoxic effects than PEG-coated AgNPs

The influence of Citrate or PEG coating on silver nanoparticle toxicity to a human keratinocyte cell line

Bastos V.[1], Ferreira de Oliveira J. M. P.[1], Brown D.[2]Jonhston H.[2], Malheiro E. [3], Daniel-da-Silva A.L.[3], Duarte I.F.[3], Santos C.[1,4*] and Oliveira H.[1]

[1]*CESAM & Laboratory of Biotechnology and Cytomics, Department of Biology, University of Aveiro, 3810-193 Aveiro, Portugal*
[2]*School of Life sciences, Heriot-Watt University, Riccarton, Edinburgh EH14 4AS, UK*
[3]*CICECO – Aveiro Institute of Materials, Department of Chemistry, University of Aveiro, Aveiro, Portugal*
[4]*Department of Biology, Faculty of Sciences, University of Porto, Rua do Campo Alegre, Porto,*

*corresponding author: csantos@fc.up.pt

Abstract

Surface coating of silver nanoparticles may influence their toxicity, in a way yet to decipher. In this study, human keratinocytes (HaCaT cells) were exposed for 24 and 48h to well-characterized 30 nm AgNPs coated either with citrate (Cit30 AgNPs) or with poly(ethylene glycol) (PEG30 AgNPs), and assessed for cell viability, reactive oxygen species (ROS), cytokine release, apoptosis and cell cycle dynamics. The results showed that Cit30 AgNPs and PEG30 AgNPs decreased cell proliferation and viability, the former being more cytotoxic. The coating molecules *per se* were not cytotoxic. Moreover, Ag+ release and ROS production were similar for both AgNP types. Cit30 AgNPs clearly induced apoptotic death, while cells exposed to PEG30 AgNPs appeared to be at an earlier phase of apoptosis, supported by changes in BAX, BCL2 and CASP-3 expressions. Concerning the impact on cell cycle dynamics, both Cit30 and PEG30 AgNPs affected cell cycle regulation of HaCaT cells, but, again, citrate-coating induced more drastic effects, showing earlier downregulation of cyclin B1 gene and cellular arrest at the G2 phase. Overall, this study has shown that the surface coating of AgNPs influences their toxicity by differently regulating cell-cycle and cell death mechanisms.

Keywords: Apoptosis, Cell cycle, Citrate-coating, Cytokines, Nanotoxicology, PEG-coating, ROS, silver nanoparticles.

1. Introduction

Silver nanoparticles (AgNPs) have very efficient antimicrobial activity, which has encouraged their widespread use in a range of applications, from medicine and industry to household and personal care products (EPA 2010) or clothing (Abdelhalim and Jarrar 2011; Behra et al. 2013; Benn and Westerhoff 2008; Eckhardt et al. 2013; Nowack et al. 2011). According to the inventory of nanotechnology-based consumer products compiled by the Project on Emerging Nanotechnologies (http://www.nanotechproject.org/cpi), ~24% of 1800 "nano" products that were introduced in the market to date are nanosilver-containing products. In face of the rapid increase in AgNP production and use, concerns about their possible impacts on the environment and human health have also grown (Nowack and Bucheli 2007). There are many routes of human exposure to AgNPs, including dermal absorption, ingestion, inhalation and injection (Ahamed et al. 2010; Chen and Schluesener 2008) and several *in vitro* studies have reported toxic effects of AgNPs towards different types of human cells (Asharani et al. 2012; Chairuangkitti et al. 2013; Foldbjerg et al. 2012; Gliga et al. 2014; Grosse et al. 2013; Hsiao et al. 2015; Jiang et al. 2013; Kang et al. 2012; Kim et al. 2009). However, the mechanisms of AgNPs-induced toxicity are still not completely understood (Browning et al. 2013). In particular, it is crucially important to determine how specific physicochemical properties, such as particle size and surface chemistry, influence AgNPs uptake, cellular fate and toxicity (Ahlberg et al. 2014; Comfort et al. 2014; Lu et al. 2010; Samberg et al. 2010).

Different properties such as NP formulation (Boonkaew et al. 2014) and size (Kim et al. 2012; Park et al. 2011), the storage environment (Ahlberg et al. 2014) and the duration of exposure (Comfort et al. 2014) have all been previously assessed in different cell types with regard to AgNPs toxic potential. However, little attention has been paid so far to the coating-dependent toxicity of AgNPs. AgNPs are frequently coated to promote stability and avoid aggregation, citrate being the most commonly used reducing agent and stabilizer (Sharma et al. 2009). Numerous polymers have also been used to coat AgNPs, such as polyvinyl pyrrolidone (PVP) (Haberl et al. 2013; Nymark et al. 2013; Wang et al. 2014), and poly(ethylene glycol) (PEG) (Fernández-López et al. 2009; Tao et al. 2007). Citrate renders NPs a negative surface charge and provides colloidal stability through electrostatic repulsions, while low molecular weight PEG can neutralize surface charge and stabilize NPs through steric hindrance. PEG coating has been reported to reduce NP reactivity (Povoski et al. 2013) and to improve penetration through the mucus layer, increasing the interest in the use of this polymer for nanomedicine purposes (Suk et al. 2011; Thorley and Tetley 2013).

The few studies which have addressed the influence of coating on AgNPs toxicity provided conflicting information. It has been reported that the charged citrate coating improved the stability of AgNPs and decreased their toxicity (Zhang et al. 2014), while other studies found that citrate-coated AgNPs could be highly cytotoxic to mammalian cells (Grosse et al. 2013;

Wang et al. 2014). On the other hand, Gliga et al. (2014) compared the cytoxicity of uncoated, PVP- and citrate-coated AgNPs in bronchial BEAS-2B cells and found no coating-dependent differences in cytotoxicity. Caballero-Díaz et al. (2013) reported that pegylation of AgNPs reduced cellular uptake and reduced the toxicity in NIH/3T3 (mouse embryonic fibroblasts), compared to AgNPs coated with other polymers. Using an *in vivo* system, England et al. (2013) demonstrated that PEG coating could "mask" the NPs from the immune system, decreasing their toxicity. However, α-methoxy-poly(ethylene glycol)-ω-mercapto (mPEG-SH)-coated AgNPs decreased viability and affected cell cycle dynamics of human liver cells (HL-7702) (Song et al. 2012). The differential effects of citrate and PEG coatings have been assessed for gold nanoparticles (AuNPs) (Brandenberger et al. 2010) in human alveolar epithelial cells (A549) cells. The authors found that the uptake of citrate-coated AuNPs by A549 cells was significantly increased compared to that of the PEG-coated AuNPs, concluding that NP surface coatings can modulate endocytic uptake pathways and cellular NP trafficking.

In this study, we aimed to compare the cytotoxic effects of AgNPs coated with citrate or PEG on human keratinocytes. Given that skin is a major entry route of AgNPs into the body, HaCaT (human keratinocyte) cells have been chosen as an *in vitro* model. Indeed, there has been evidence that AgNPs with diameters in the 20-40 nm range can penetrate skin *in vivo* and be detected in deeper layers (George et al. 2014; Larese et al. 2009). HaCaT cells were exposed to citrate- and PEG-coated AgNPs of 30 nm (Cit30 and PEG30, respectively) and the effects on cell viability, intracellular ROS production, cytokines expression, apoptosis induction and cell cycle profile were assessed after 24 and 48 h. Putative toxicity of the coatings alone was also investigated.

2. Material and methods

2.1. Chemicals

Sterile, purified and endotoxin-free silver nanoparticles (Biopure AgNPs 1.0 mg/mL in water), with a diameter of 30 nm and a citrate or polyethyleneglycol (PEG) surface, designated as Cit30 and PEG30, respectively, were purchased from Nanocomposix Europe (Prague, Czech Republic). Citric acid ($C_6H_8O_7.H_2O$) was purchased from Sigma Aldrich (St. Louis, Missouri, USA); Poly(ethylene glycol) PEG (Mw 5 kDa) from Laysan Bio® (Arab, Alabama, USA) . Dulbecco's modified Eagle's medium (DMEM), fetal bovine serum (FBS), antibiotics and phosphate buffer saline (PBS, pH 7.4) were purchased from Life Technologies (Carlsbad, CA, USA). 3-(4,5-dimethylthiazol-2-yl)-2,5-diphenyltetrazolium bromide (MTT), dimethyl sulfoxide (DMSO), dichlorodihydrofluorescein diacetate (DCFH2-DA), propidium iodide (PI), RNase and DNase I were obtained from Sigma-Aldrich (St. Louis, MO, USA). FITC Annexin V Apoptosis Detection Kit (BD Pharmingen, San Diego, CA-USA); RNeasy Mini Kit columns was from Qiagen, Hilden, Germany; Omniscript RT Kit from Qiagen, Hilden, Germany; and iQ

SYBR Green Supermix from BioRad, Hercules, CA-USA.

2.2. Physicochemical characterization of AgNPs

The morphology and size of AgNPs was assessed by scanning transmission electron microscopy (STEM, Hitachi SU-70 (Hitachi High-Technologies Europe GmbH, Germany) operating at 30 kV. Samples for STEM analysis were prepared by evaporating dilute suspensions (concentration) of the nanoparticles on a copper grid coated with an amorphous carbon film. The hydrodynamic diameter and polydispersity index (PdI) of the nanoparticles were measured by dynamic light scattering (DLS) and the zeta potential was assessed by electrophoretic mobility, both measurements using a Zetasizer Nano ZS (Malvern Instruments, UK).

Silver quantification measurements were performed by inductively coupled plasma optical emission spectrometry (ICP-OES) in an Activa M Radial spectrometer (Horiba Jobin Yvon, France), employing a charge coupled device (CCD) array detector, with a wavelength range of 166–847 nm and radial plasma view. Samples were introduced into the ICP plasma using an HF resistant sample introduction system including a Burgener nebulizer, a cyclonic spray chamber and a quartz torch with aluminium injector. Samples for ICP-OES were prepared by addition of 10 µL AgNPs (1.0 mg/mL) to 990 µL of either ultrapure water or complete culture medium, incubation for variable periods (0, 4, 24 or 48h), followed by centrifugation at 40000 rcf for 120 min at 4ºC (in accordance with the manufacturer's recommendations) to deposit the nanoparticles and separate the supernatant (with dissolved ionic silver). Acid digestion of the supernatant was then performed by mixing 500 µL with 100 µL of acids ($HCl:HNO_3$ 2:1 v/v) and 400 µL of ultrapure water. The % dissolution of AgNPs to ionic silver was calculated as $100 \times F \times [Ag]/Ci$, where F is the dilution factor, Ci the initial concentration of AgNPs (based on the stock solution concentration, indicated by the manufacturer) and [Ag] the concentration of silver determined by ICP-OES.

2.3. Cell Culture

The HaCaT cell line, a nontumorigenic immortalized human keratinocyte cell line (Boukamp et al. 1988), was obtained from Cell Lines Services (Eppelheim, Germany). Cells were grown in complete medium, (Dulbecco's modified Eagle's medium, supplemented with 10% fetal bovine serum (FBS), 2 mM L-glutamine, 100 U/mL penicillin, 100 µg/mL streptomycin and 250 µg/mL fungizone) at 37 °C in 5% CO_2 humidified atmosphere. For each experiment, cells were seeded at a concentration 60000 cells/mL in 96 well plates, and allowed to adhere for 24 h and then medium was replaced with fresh medium containing citrate- or PEG-coated AgNPs. Depending on the experiment, the silver ion and the coating agent *per se*, dissolved in complete medium, were used as controls. The effects were measured after 24 and 48 h.

185 *2.4. Exposure and Viability assay*

186 Cell viability was determined by the colorimetric 3-(4,5- dimethyl-2-thiazolyl)-2,5-diphenyl
187 tetrazolium bromide (MTT) assay (Twentyman and Luscombe 1987). Cells were seeded in 96-
188 well plates and cultured as described above. Cell viability was assessed in cells exposed to free
189 citrate and PEG (same Mw as PEG in AgNPs coating) at concentrations below the maximum
190 quantity added at the time of NP synthesis (before wash process), which was 2 mM for citrate
191 (~378 µg/mL) and 200 µg/mL for PEG (information provided by the manufacturer
192 Nanocomposix). Cells were exposed to citrate or PEG dissolved in complete culture medium at
193 0, 50, 100, 200, 300, 350 and 400 µg citrate/mL, and 0, 6, 12.5, 25, 50, 100 and 200 µg
194 PEG/mL. Silver nitrate was dissolved in complete medium at concentrations of 0, 0.2, 0.5, 1,
195 2.5, 5, 7.5, 10 and 50 µg Ag^+/mL. Cells were exposed to citrate- or PEG-coated AgNPs at
196 concentrations of 0, 0.5, 5, 10, 25, 50, 75 and 100 µg/mL. Cell viability was measured after 24
197 h, but in the case of Ag+ and coated AgNPs a 48h exposure was also assayed. Fifty microliters
198 of MTT (1 mg/mL) in phosphate buffered saline (PBS) was then added to each well, and
199 incubated for 4h at 37 °C, 5% CO_2. Medium was then removed and 150 µL of DMSO were
200 added to each well to solubilize the formazan crystals.
201 The optical density of reduced MTT was measured at 570 nm in a microtiter plate reader
202 (Synergy HT Multi-Mode, BioTeK, Winooski, VT), and the relative cell metabolic activity
203 (MA) (calculated as a % with respect to control cells) was calculated as: MA = [(Sample Abs –
204 DMSO Abs) / (Control Abs – DMSO Abs)]*100. Three independent assays were performed
205 with at least 2 technical replicates each and the results compared with the control (no exposure).
206 From the MTT results, the IC50 for citrate coated AgNPs (the most cytotoxic) was 40 µg/mL
207 and 37.4 µg/mL at 24 and 48 h respectively. Therefore, the concentrations of coated AgNPs
208 corresponding to IC50 and IC20 (40 µg/mL and 10 µg/mL, respectively) were selected for the
209 following assays, for the silver ion, the IC50 was 1.26 µg/mL and in that case a concentration
210 which didn't cause significant cytotoxicity (0.8 µg/mL) was selected. This concentration was
211 higher than the Ag^+ concentration released from citrate-coated AgNPs at time 0h (3.77% in 10
212 µg/mL of citrate- AgNPs, which corresponds to 0.377 µg/mL of Ag^+), but was a dose that did
213 not cause significant cytotoxicity through MTT assay.
214
215 *2.5. Uptake potential by flow cytometry*

216 Uptake potential of Cit30 and PEG30 by HaCaT cells was assessed by flow cytometry (FCM)
217 as previously described by Suzuki et al (2007). Briefly, cells were seeded in 6-well plates and
218 after AgNPs exposure they were trypsinized, collected to FCM tubes and analyzed by FCM.
219 Both parameters, forward scatter (FS), which give information on the particle's size, and side
220 scatter (SS), information on complexity of particles, were measured in a Coulter XL Flow
221 Cytometer (Beckman Coulter, Hialeah, FL-USA) equipped with an argon laser (15 mW, 488

nm). Acquisitions were made using SYSTEM II software v. 3.0 (Beckman Coulter, Hialeah, FL). For each sample, 5000–20000 cells were analyzed at a flow rate of about 1000 cells/s.

2.6. Intracellular ROS Formation

Intracellular ROS production was assessed by flow cytometry (FCM) with the use of dichlorodihydrofluorescein diacetate (DCFH2-DA) as a fluorescent probe. This probe enters the cells and is deacetylated by cellular esterases producing non-fluorescent DCFH2 and diacetate. In the cytosol DCFH2 is quickly oxidized to fluorescent DCF by intracellular ROS. Cells were seeded in 6-well plates at a concentration of 60000 cells/mL and after AgNPs exposure for 24h, medium was discarded and cells were incubated for 30 min, at 37ºC, in the dark with serum-free DMEM containing 10 mM DCFH2-DA. Cells were washed with PBS, trypsinised and collected for analysis. Acquisitions were made using a Coulter EPICS XL flow cytometer (Coulter Electronics, Hialeah, Florida, USA) equipped with an argon laser (15 mW, 488 nm). Acquisitions were made using SYSTEM II software v. 3.0 (Beckman Coulter, Hialeah, FL). ROS formation was estimated from the median fluorescence intensity (MFI) of DCF using the FlowJo software (Tree Star Inc., Ashland, OR-USA). For each sample, the number of events reached at least 10000.

2.7. Cytokine estimation using cytometric bead array

Cytokine production was assessed using Bioplex kits. Briefly, the cell supernatants (removed, centrifuged and frozen at -80ºC) were used to estimate the release of the following cytokines from treated cells: interleukin-1 beta (IL-1β), IL-6, tumour necrosis factor-alpha (TNF-α), IL-10 and monocyte chemoattractant protein-1 (MCP-1). Lipopolysaccharide (LPS) was used as a positive control. Bead array kits were obtained from Beckton Dickinson (Oxford, UK) and a master mix prepared according to the manufacturer's instructions. The master mix was incubated with each of the test supernatants for 1 h, followed by the addition of detection beads and incubated for a further 2 h at room temperature. The beads were then washed in wash buffer and analyzed using a BD^{TM} FACS array flow cytometer which had previously been set up and calibrated using standard beads for each cytokine under investigation.

2.8. Annexin V assay

Apoptosis and cell viability were measured by flow cytometry (FCM) in a Coulter XL Flow Cytometer (Beckman Coulter, Hialeah, FL-USA), through the FITC Annexin V Apoptosis Detection Kit, according to manufacturer. Briefly, cells were detached and washed with PBS, and the cells resuspended in diluted binding buffer provided with the kit (1:10 in distilled water) at 1×106 cells/ml. To stain the cell suspension, 5µL of FITC-Annexin V and 5µL of PI were added for 15 min at room temperature in the dark, after which each sample was diluted in

400µL binding buffer. For each sample, 10000 events were analyzed and the percentages were calculated from the number of cells in each quadrant divided by the total number of cells.

2.9. Gene expression of apoptosis related genes

Total RNA of control and exposed cells was extracted using the TRIzol method. Organic phase separation was achieved in Phase-Lock Gel Heavy tubes (5 Prime 3 Prime, Inc., Boulder, CO). The aqueous phase was mixed with 1 vol 70% ethanol and RNA was purified using RNeasy Mini Kit columns. Synthesis of cDNAs was performed by a reverse transcriptase (RT) reaction: 2 µg total RNA were pre-incubated with DNase I and reverse-transcribed with 1 µM Oligo dT18, using the Omniscript RT Kit. The cDNA samples were prediluted in ultrapure MilliQ water (1:20). The final individual qPCR reactions contained iQ SYBR Green Supermix, 150nM each gene-specific primer and 1:4 (v/v) prediluted cDNA (1:20). Primers were designed using the program Primer3 (Rozen and Skaletsky 2000) and confirmed for specificity by the UCSC In-Silico PCR Genome Browser (http://genome.ucsc.edu/cgi-bin/hgPcr). The qPCR program included 1 min denaturation at 95 °C, followed by 40 cycles at 94 °C for 5 s, 58 °C for 15 s, and 72 °C for 15 s. After qPCR, a melting temperature curve was performed. At least two technical replicates per sample of qPCR were used from each of three independent biological replicates. Average PCR and cycle thresholds were determined from the fluorescence data using the algorithm Real-Time PCR Miner (Zhao and Fernald 2005). Gene expression of *BAX*, *BCL2*, *CASP3* were normalized with the *GAPDH* reference gene and expressed relative to control cells, calculated from the average efficiencies and cycle thresholds using the Pfaffl method (Pfaffl 2001).

2.10. Cell cycle

Cell cycle was analyzed by flow cytometry according to the method previously described (Oliveira et al. 2014). Briefly, cells were seeded in 6-well plates and after exposure they were washed with PBS, harvested using Trypsin-EDTA and centrifuged twice at 300 x*g* for 5 min. Cells were then fixed with 85% cold ethanol and kept at -20 ºC until analysis. At the time of analysis cells were centrifuged at 300 *g* for 5 min, resuspended in PBS and filtered through a 35-µm nylon mesh to separate aggregates. Then, 50 µL RNase (1mg/mL) and 50 µL propidium iodide (PI) (1mg/mL) were added to each sample which were then incubated for 20 min in darkness at room temperature until analysis. The relative fluorescence intensity of the stained nuclei was measured in a Coulter XL Flow Cytometer. For each sample, the number of nuclei analyzed was approximately 5,000. The percentage of nuclei in each phase of the cell cycle (G0/G1, S and G2 phases) was analyzed using the FlowJo software **(**Tree Star Inc., Ashland, Oregon, USA).

296 *2.11. Gene expression of cell cycle related genes*

297 Total RNA extraction and cDNA synthesis were performed as described above. Gene
298 expression of cyclin B1 (*CCNB1*), cyclin E1 (*CCNE1*), cyclin-dependent kinase 1 (*CDK1*) and
299 cyclin-dependent kinase 2 (*CDK2*) were normalized with the *GAPDH* reference gene and
300 expressed relative to control cells, calculated from the average efficiencies and cycle thresholds
301 using the Pfaffl method (Pfaffl 2001).
302
303 *2.12. Statistical analysis*

304 The results are reported as mean ± standard deviation (SD) of 2 technical replicates in each of
305 the 3 independent experiments. For MTT assay, the statistical significance between control and
306 exposed cells was performed by one-way ANOVA, followed by Dunnet and Dunn's method (as
307 parametric and non-parametric test, respectively), using Sigma Plot 12.5 software (Systat
308 Software Inc.). For the other assays, results were compared using two-way ANOVA, followed
309 by Holm-Sidak test using also Sigma Plot 12.5 software (Systat Software Inc.). The differences
310 were considered statistically significant for $p < 0.05$. Principal Component Analysis (PCA) was
311 used to perform multivariate analysis. All multivariate analyses in this paper were carried out
312 using the Canoco for Windows vs 4.5.
313
314 **3. Results**

315 *3.1. Physicochemical characterization of AgNPs dispersed in water and in cell culture*
316 *medium*

317 Scanning transmission electron microscopy (STEM) images (Figure 1) showed that AgNPs
318 were mainly spherical in shape with a mean diameter of 27.1 ± 3.0 nm and 27.7 ± 3.2 nm, for
319 citrate and PEG coated nanoparticles respectively, and with a narrow size distribution. The
320 hydrodynamic diameter (Z-average size) in water was above the primary particle size (Table 1),
321 especially in the case of PEG30 NPs, as expected based on the larger volume of PEG molecules
322 compared to citrate. The values of polydispersity indexes (PdI) were below 0.3, thus indicating
323 monodisperse distributions. As to the zeta potential, citrate-stabilized NPs carried a strong
324 negative surface charge (ζ -42.7 ± 2.7 mV), while the surface of the PEG-stabilized NPs was
325 less negative (ζ -12.1 ± 0.5 mV, Table 1). The amount of dissolved ionic silver in ultrapure
326 water suspensions of Cit30 and PEG30 AgNPs was 3.32 ± 0.04% and 0.63 ± 0.01%,
327 respectively.
328 Regarding the behavior of AgNPs in cell culture medium (DMEM with 10% FBS), Cit30
329 AgNPs increased their hydrodynamic diameter, as soon as they were suspended in the medium
330 and progressively over time up to 93.7 nm after 48h (Figure 2a), possibly reflecting the
331 formation of a protein corona. Additionally, the zeta potential (ζ) increased from -42.7 ± 2.7 in

water to -8.5 ± 0.4 mV in the cell culture medium, indicating a less negative surface, hence lower electrostatic repulsions. The release of ionic silver (Ag^+) increased to 7.6 ± 0.1% at 48h, which corresponds to an absolute concentration of 0.77 µg/mL Ag+ (Figure 2b). PEG30 AgNPs showed a more stable hydrodynamic diameter over incubation time, likely because PEG was not as readily displaceable as citrate by the medium proteins. The dissolution behavior of PEG30 AgNPs was very similar to that of Cit30 AgNPs, reaching identical ionic silver concentrations at 48h (Figure 2b).

3.2. Effects on cell growth and morphology

HaCaT cells in control conditions (exposed to cell culture medium) showed typical morphology (Supplementary Figure S1 a, f). When cells were exposed to Cit30 AgNPs for 24 and 48 h, their confluence decreased, especially at the highest concentration tested (40 µg/mL) (Supplementary Figure S1 c, h). Compared to Cit30 AgNPs, PEG30 AgNPs induced a lesser decrease in cell confluence, which was only visible after 48 h (Supplementary Figure S1 j). No visible morphological alterations were detected at 24 h for Cit30 NPs.

3.3. Cell Viability

The viability of HaCaT cells was negatively affected by AgNPs coated either with citrate or with PEG, although to different extents (Figure 3a-b). Upon exposure to Cit30 AgNPs at concentrations higher than 25 µg/mL and 50 µg/mL cell viability was significantly reduced after 24 h and 48 h. Furthermore, Cit30 AgNPs at concentrations higher that 50 µg/mL reduced cell viability to $\leq$ 20% even after 24 h. In contrast, PEG30 AgNPs, decreased cell viability significantly from concentrations >25 µg/mL, but only after 48 h. The viability results were also expressed using surface area as dose metrics, instead of mass concentration. The curves obtained (Supplementary Figure S2) actually had very similar profiles to those shown in Figure 3a-b, indicating that surface area was not determinant for the different toxicity of the two AgNP types.

In order to investigate potential inherent toxicity of the coating substances, the viability of cells upon exposure to citrate and PEG (in the same Mw as in AgNP coating) was assessed (Figs. 3c-d). Citrate induced a significant decrease in cell viability at concentrations above 100 µg/mL. However, the concentrations of citrate that corresponded to the administered AgNPs doses were well below this value (at 100 µg/mL of Cit30 AgNPs the maximum citrate concentration is 37,8 µg/mL (*Nanocomposix*® information)), thus not accounting for the observed toxicity of Cit30 AgNPs. In the case of exposure to PEG, the viability did not decrease significantly for any of the concentrations tested.

3.4. Uptake potential by flow cytometry

The uptake of both Cit30 and PEG30 AgNPs at 24h was determined by quantitative analysis of the intracellular side scatter signal by flow cytometry (Figure 4). Both concentrations (10 and 40 μg/mL) induced an increase in the uptake potential of Cit30 AgNPs by HaCaT cells, while for PEG30 an increase in the uptake potential was only observed for the highest concentration (40 μg/mL). Overall, the results suggest that PEG30 AgNPs are taken up by HaCaT cells to a lower extent than Cit30 AgNPs.

3.5. Intracellular ROS Formation

The quantification of intracellular ROS in HaCaT cells exposed to AgNPs for 24h is presented in Figure 5. Both Cit30 and PEG30 AgNPs induced the production of ROS reaching a significant 1.2 fold increase at the highest dose tested (40 μg/mL), compared to control cells. The ROS levels were similar for the two NP types.

3.6. Inflammatory Cytokine release

Significant differences in cytokine release upon AgNPs exposure were noted only for MCP-1, while there was no effect on the other cytokines studied (IL-1β, IL-6, IL-10 and TNF-α) (data not shown). The results regarding the release of MCP-1 by HaCaT cells treated with Cit30- and PEG30 AgNPs are shown in Figure 6. While LPS, used as positive control, induced a significant increase in MCP-1 release at 48h, both Cit30 and PEG30 AgNPs induced a significant decrease compared to control cells.

3.7. Annexin V assay

The potential of AgNPs to induce apoptosis in HaCaT cells was assessed by the Annexin V-FITC/PI assay. As shown in Figure 7 a-b, Ci30 AgNPs decreased the percentage of intact cells (not significantly for 48h exposure to the highest concentration of 40 μg/mL and increased the percentage of dead cells, especially at 24h exposure to the high concentration. Concerning early apoptosis, the results showed a significant increase after 48 h exposure to 40 μg/mL Cit30 AgNPs, while the percentage of cells at late apoptosis/necrosis was increased for all conditions (not significantly for 48h exposure to the low concentration) In contrast, the exposure of HaCaT cells to PEG30 AgNPs did not induce any significant changes in the apoptosis profile for neither periods or NP concentrations (Figure 7 c-d).

3.8. Gene Expression of apoptosis related genes

Apoptosis was evaluated at transcriptional level by the analysis of the expression of apoptosis related genes BAX, BCL2 and CASP3 (Figure 8). In cells exposed to Cit30 AgNPs, there was a trend for BAX expression to be upregulated, reaching statistical significance at low

concentration (10 µg/mL) 24h exposure and at high concentration (40 µg/mL) 48 h exposure. Moreover, BCL2 was found to be upregulated at 48h exposure to high concentration of Cit30 AgNPs. On the other hand, the three genes showed consistent upregulation in cells exposed to PEG30 AgNPs. The statistical comparison between Cit30 and PEG30 AgNPs exposed cells showed that for both times and concentrations the expression level of the three selected genes was significant lower in cells exposed to Cit30 AgNPs.

3.9. Cell cycle and clastogenicity

Figure 8 shows the effect of Cit30 and PEG30 AgNPs on the cell cycle of HaCaT cells. Cit30 AgNPs in both doses induced a decrease in the percentage of cells in G0/G1 and an increase in the percentage of cells in G2, this effect being visible for both periods, but more pronounced at 48 h ($p < 0.01$) (Figure 9a). As for PEG30 AgNPs, in addition to a decrease in the number of cells in G0/G1 and a slight increase in cells at G2 there was a significant increase in the number of cells in S phase An example of the histograms obtained after 40 µg/mL Cit30 and PEG30 AgNPs exposure during 48 h are shown in Supplementary Figure S3.

3.10. Expression of cell cycle related genes

Exposure to AgNPs significantly changed the expression levels of selected genes involved in cell cycle regulation (Figure 10). Exposure to Cit30 AgNPs downregulated the expression of cyclin B1 gene (*CCNB1*) for 40 µg/mL at both time points. For PEG30 AgNPs *CCNB1*, expression was decreased for 40 µg/mL only at 48 h exposure. The expression of the *CDK2* gene, for cells exposed to citrate- AgNPs was increased for 40 µg/mL at 24 h and decreased at 48 h for the same concentration. The expression of the other genes tested was not significantly altered upon exposure to AgNPs.

4. Discussion

In this work, we have investigated the cellular effects of well-characterized AgNPs with different coatings (citrate and PEG) but the same nominal diameter (30 nm), in order to address the influence of NP surface coating on biological outcomes in keratinocytes, assessing, among other endpoints, less commonly reported changes in cell cycle dynamics. Further motivation for testing the toxicity of these NP types arose from the growing interest in using PEG-coated NPs in nanomedicine applications (Jokerst et al. 2011) and the widespread use of citrate coating in AgNPs synthesis (Zhang et al. 2011), thus making it timely and useful to report on the cytotoxic effects of such particles.

The characterization results revealed that AgNPs exhibited different time-course behavior in culture medium, depending on the coating surface. The hydrodynamic diameter of Cit30 AgNPs increased immediately after suspension in culture medium, which is in agreement with previous

observations (Wang et al. 2014) and is likely to be due to the formation of a protein corona, as reported for metal nanoparticles (Casals et al. 2010; Maiorano et al. 2010). Moreover, some aggregation induced by the high ionic strength of the culture medium may also have occurred (El Badawy et al. 2012; Li et al. 2012; Robert 2010). Conversely, the hydrodynamic diameter of PEG30 AgNPs did not show significant variation in culture medium indicating high colloidal stability, which is likely to derive from steric repulsions (Caballero-Díaz et al. 2013), and lower propensity for the PEG coating molecules to be displaced by proteins (Michel et al. 2005).

In terms of cell viability, evaluated through the MTT mitochondrial activity assay, Cit30 AgNPs were found to be more cytotoxic than PEG30 AgNPs. Although, to our knowledge, the direct comparison between these two NP types hasn't been previously reported, Wang et al. (2014) found a significant decrease in the viability of bronchial BEAS-2B cells upon 24h exposure to 20 nm citrate-coated AgNPs at 6.25-50 μg/mL, while Song et al. (2012) showed PEG-coated AgNPs to cause significant viability decreases in human liver cells (HL-7702) at concentrations as low as 6.25 μg/mL. Differences in NP properties (e.g. size and surface area) as well as cell type-dependent effects (e.g. uptake) may account for the discrepancy in relation to our results. The coating substances *per se* were not responsible for the larger cytotoxicity hereby found for Cit30 NPs compared to PEG30 NPs, as neither of them decreased cell viability at the concentrations present when AgNPs were administered to cells. Also, Cit30 and PEG30 NPs showed similar dissolution behavior in culture medium, thus extracellular Ag+ could not justify the difference in the toxicity of the two NP types. Accordingly, Gliga and co-workers (Gliga et al. 2014) have shown that AgNPs supernatants, containing ionic silver, did not affect cells. On the other hand, the intracellular release of Ag+ following cellular uptake (sometimes called the Trojan horse effect) has been proposed by several authors (Hsiao et al. 2015; Park et al. 2010) to be greatly responsible for AgNPs toxicity. Thus, it is possible that the different coatings used in our study influenced cytotoxicity indirectly, by modulating the interaction of NPs with cells, namely the extent of NP uptake and intracellular release of Ag+.

To quantitatively evaluate the cellular uptake of AgNPs we have used flow cytometry and related the increase in side scatter (SS) intensity with an increase in intracellular AgNPs, as previously described (e.g. Greulich et al. 2011, Zucker et al. 2013). The obtained data suggested that PEG30 AgNPs were taken up by cells to a lower extent than Cit30 AgNPs, which could justify the lower cytotoxic potential of the former particles. Concordantly, Caballero-Díaz et al (2013) showed that pegylation of polymer-coated AgNPs reduced cellular uptake and toxicity to mouse embryonic fibroblasts (NIH/3T3 cells). Furthermore, it can be postulated that thiolated PEG may complex Ag+ ions and lower their bioavailability and toxicity, as proposed for PVP-coated AgNPs (Wang et al. 2014). Also, when evaluating the uptake rates of gold NPs on human alveolar epithelial cells (A549), Brandenberger et al (2010) observed that significantly more plain NPs (i.e., stabilized with citrate buffer) could enter the cells than PEG-coated gold

NPs.

ROS can be generated either by a direct pro-oxidant effect of the NP or endogenously upon interaction with cellular material. In our work, both NP types caused a similar increase in intracellular ROS, supporting ROS-induced cytotoxicity, although not explaining the higher toxicity of Cit30 compared to PEG30 AgNPs. Enhanced ROS production has been often highlighted as a major cause for AgNP toxicity in several cell types (Kim and Ryu 2013), although it has also been reported, in human liver and colon cells, that AgNPs could cause cytotoxicity without oxidative stress (Sahu et al. 2014). Furthermore, Chairuangkittia et al. 2013 described that the toxicity of AgNPs to A549 was due both to ROS dependent and independent pathways, the latter related with cell cycle arrest. Our results show that both AgNPs induce arrest in cell cycle at 24h with more drastic effects for Cit30 at 48h. In fact, in previous studies from our group (Carrola et al. 2016) the cell metabolic profile of HaCaT cells exposed to the same Cit30 AgNPs was evaluated and an increase in GSH was detected, suggesting the triggering of a protective mechanism against ROS-induced oxidative damage, which is consistent with the strong antioxidant capacity of this cell line (Mukherjee et al 2012). Therefore, from our results we can hypothesize that the induction of ROS is one of several mechanisms of AgNP induced toxicity in HaCaT cells. Further studies are needed to clarify how the different coatings modulate ROS dependent and independent pathways of AgNPs induced toxicity.

Regarding cytokine release, the only significant effect was a decrease in MCP-1 production compared to control cells, caused in similar extent by Cit30 and PEG30 NPs. Other cytokines, namely IL-1β, IL-6, IL-10 and TNF-α did not vary upon AgNPs exposure. These results are comparable to those reported by Orlowski et al. (2013), where AgNPs coated with tannic acid led to a decrease of MCP-1 and non-relevant changes in the IL family. However, the same study reported an increase of MCP-1 in murine monocytes and keratinocytes after exposure to unmodified AgNPs, showing that coating can influence the inflammatory response to AgNPs. Oppositely to our results, increases in cytokines release have also been reported by others (Suliman Y et al. 2015; Yang et al. 2012); different cell types as well as different properties of the AgNPs tested may account for the discrepancies observed. Also, adsorption of cytokine proteins onto the NP surface may have occurred contributing to a decrease in protein function (Brown et al. 2010).

Apoptosis and necrosis results showed that Cit30 AgNPs increased the number of necrotic cells, as well as early and late apoptotic cells. A slight increase of apoptotic and necrotic A549 cells after exposure to citrate-stabilized AgNPs has also been reported by Foldbjerg et al. (Foldbjerg et al. 2012). On the other hand, PEG30 AgNPs did not significantly influence these populations, although a trend to increase early-apoptotic cells was seen, in agreement with the results reported by Zhang and co-workers (2015) for male somatic Leydig (TM3) and Sertoli (TM4)

cells. Interestingly, in the present work, the expression of apoptosis-related genes was also found to differ between Cit30 and PEG30 NPs. In particular, PEG30 AgNPs increased the expression of *BAX* (pro-apoptotic), *BCL-2* (anti-apoptotic) and *CASP-3* genes at both concentrations and time points. Piao and co-workers (2011) observed that AgNPs induced a mitochondria-dependent apoptotic pathway via modulation of *BAX* and *BCL-2* expressions, resulting in the disruption of mitochondrial membrane potential, followed by cytochrome c release from the mitochondria and activation of caspases 9 and 3. Furthermore, Jeyaraj and co-workers (2015) found an upregulation of *BAX*, caspases-6 and -9 and downregulation of *BCL-2*. In our study, both *BCL-2* and *BAX* and of the effector *CASP-3* were upregulated, particularly by PEG30 AgNPs, supporting that these NPs were more prone to induce intrinsic apoptosis than Cit30 NPs. This difference between the two NP types concerning the effects on apoptotic/necrotic cells and on the transcripts of apoptotic-related genes strongly suggests that, when exposed to PEG30 AgNPs, HaCaT cells may cope with the apoptotic cascade at the early stage, promoting apoptotic and antiapoptotic expression and resulting in lower cytotoxicity. The upregulation of *BCL-2* by PEG30 AgNPs was particularly relevant. Belonging to the anti-apoptotic protein family, it performs its anti-death function by sequestering monomeric *BAX* and *BAK*. It is known that certain cancer cells depend upon *BCL-2* and other anti-apoptotic proteins for survival (Brunelle and Letai 2009). In contrast, Cit30 AgNPs seemed to act mainly at a necrotic level and, in the cells undergoing apoptosis, this will lead to cell death. Overall, our data showed that Cit30 and PEG30 AgNPs differed in the way they induced apoptosis, with the former leading to necrotic/late apoptotic processes, and the latter stimulating both apoptotic and anti-apoptotic transcripts, which may modulate cells apoptotic response at the early stage. This influence of NP coating on the apoptotic/necrotic mechanisms was also evidenced by the PCA analyses (Figure 11).

Both Cit30 and PEG30 AgNPs were found to induce changes on the cell cycle dynamics of HaCaT cells. In particular, Cit30 AgNPs induced a significant increase in the percentage of cells in G2, indicating an arrest at this phase, visible for both concentrations and time periods, while the PEG30 AgNPs induced an increase in the number of cells in S phase, more visible at 24 h, pointing to an S phase delay. The cell cycle arrest in G2/M phase after exposure to NPs was previously related to DNA damage repair (AshaRani et al. 2009). Indeed, in another report, we have presented data showing that Cit30 AgNPs induced DNA damage and micronucleus (MNi) formation, increased mononucleated cells, and decreased binucleated cells and the nuclear division index, thus pointing to clear cytostatic effects even at a low dose (~IC20) and after a short period of exposure (24 h) (Bastos et al, 2016, manuscript submitted). Cell cycle arrest at G2 as a result of AgNP exposure was previously observed by others (AshaRani et al. 2009; Kang et al. 2012; Lee et al. 2011; Wei et al. 2010). For instance, Song et al. (2012) found an increase in the percentage of liver cells at the G2/M phase upon 24h exposure to 100 μg/mL

mPEG-SH coated AgNPs. Also, Foldbjerg et al. (2012) found that PVP-coated AgNPs significantly increased the percentage of A549 cells in G2/M and S phases. S phase delay was also observed by Liu et al. (2010) in HepG2 cells exposed to PVP-coated AgNPs. Furthermore, an increase in the sub-G1 population of cells (which may indicate apoptosis) was reported by Jiang et al. (2013) in CHO-K1 cells exposed to BSA-coated AgNPs and by Chairuangkitti et al. (2013) in A549 cells exposed to 200 µg/mL AgNPs. Li et al. (2013) reported cell cycle arrest at G0/G1 phase and a shortened S phase after only 8 h of AgNPs exposure, showing that AgNPs may interfere in cell cycle regulation at different checkpoints. In the present work, we have also assessed the expression of selected cell cycle regulator genes. Exposure to Cit30 AgNPs at 40 µg/mL for 24 and 48h induced downregulation of *CCNB1*, while for PEG30 AgNPs, the expression of *CCNB1* was only significantly decreased after exposure for 48 h. Cyclin B1, encoded by the *CCNB1* gene, is a regulatory protein which complexes with *CDK1*, both playing a determinant role in G2/M phase transition of the cell cycle. In general, our results agree with the study of Foldbjerg and co-workers (2012), where they found downregulation of *CCNB1* and *CDK1* for the A549 cell line exposed to AgNPs during 24 and 48 h. Furthermore, we found a statistically significant difference between the two NP types for the expression of *CCNE1*. Cyclin E1, encoded by the *CCNE1* gene, forms a complex with *CDK2*, which accumulates at the G1-S phase and is degraded as cells progress through the S phase. *CCNE1* expression was generally lower upon exposure to PEG30 compared to Cit30 exposure, which agrees with the increase in the percentage of cells in S phase observed for PEG30 AgNPs. AshaRani et al. (2012) also reported downregulation of *CCNB1* and *CCNE1* genes in lung and brain cells exposed to AgNPs. In summary, as corroborated by the PCA analysis (Figure 10), coating influenced the way that AgNPs interfered with the cell cycle, with Cit30 AgNPs leading to an impairment of the MPF (maturation promoting factor) complex and blocking cells in G2, and PEG30 AgNPs leading to a delay in the S-phase. Impacts on cell cycle are not routinely assessed for NPs, and we suggest that this response is tested for a wider range of NPs and cell types in the future.

5. Conclusions

In summary, this study demonstrates that the widely used citrate-coated AgNPs decreased the viability of HaCaT cells more severely than PEG-coated AgNPs. This difference was not due to putative effects of the coating molecules *per se* (as they produced no cytotoxicity), neither to the extent of extracellular release of ionic silver or the amount of ROS produced, as they were similar for both NP types. The differently coated AgNPs produced, however, distinct effects regarding the mode of cell death and cell cycle progression. While Cit30 AgNPs clearly induced apoptotic/necrotic death, cells exposed to PEG30 AgNPs appeared to be at an earlier phase of apoptosis mechanisms, as supported by gene expression analysis. With regard to the impact on

cell cycle progression, both Cit30 and PEG30 AgNPs affected cell cycle regulation of HaCaT cells, but, again, citrate-coating induced more severe effects, showing earlier downregulation of the cyclin B1 gene and blockage of cells at G2. Considering that AgNPs are present in a vast number of consumer products, it is important to determine if or which NPs are more cytotoxic. This study suggests that PEG-coating can be regarded as a good alternative to citrate stabilization of AgNPs used in industrial and medical applications, where it is important to reduce the toxicity towards human skin cells. The applicability of these findings to other cell types needs to be investigated in future studies.

Acknowledgments

This work was developed in the scope of the projects CICECO-Aveiro Institute of Materials (Ref. FCT UID/CTM/50011/2013) and CESAM (Ref. FCT UID/AMB/50017/2013), financed by national funds through the FCT/MEC and when applicable co-financed by the European Regional Development Fund (FEDER) under the PT2020 Partnership Agreement. Funding to the project FCOMP-01-0124-FEDER-021456 (Ref. FCT PTDC/SAU-TOX/120953/2010) by FEDER through COMPETE and by national funds through FCT, and the FCT-awarded grants (SFRH/BD/81792/2011; SFRH/BPD/48853/2008; SFRH/BPD/74868/2010) are acknowledged. I.F.D and A.L.D.S. acknowledge FCT/MCTES for the research contracts under the Program 'Investigador FCT' 2014. Authors acknowledge Tiago Pedrosa for the technical assistance in MTT assay and ROS assessment.

References

Abdelhalim MAK, Jarrar BM. Renal tissue alterations were size-dependent with smaller ones induced more effects and related with time exposure of gold nanoparticles. Lipids Health Dis. 2011; 10.

Ahamed M, Alsalhi M, Siddiqui M. Silver nanoparticle applications and human health. Clin Chim Acta. 2010; 411.23: 1841-1848.

Ahlberg S, Meinke MC, Werner L, Epple M, Diendorf J, Blume-Peytavi U, Lademann J, Vogt A, Rancan F. Comparison of silver nanoparticles stored under air or argon with respect to the induction of intracellular free radicals and toxic effects toward keratinocytes. Eur J Pharm Biopharm. 2014; 88.3: 651-657

AshaRani P, Low Kah Mun G, Hande M, Valiyaveettil S. Cytotoxicity and genotoxicity of silver nanoparticles in human cells. ACS Nano. 2009; 3:279-290.

Asharani P, Sethu S, Lim H, Balaji G, Valiyaveettil S, Hande M. Differential regulation of intracellular factors mediating cell cycle, DNA repair and inflammation following exposure to silver nanoparticles in human cells. Genome Integr. 2012; 3.1: 2.

Behra R, Sigg L, Clift M, Herzog F, Minghetti M, Johnston B, Petri-Fink A, Rothen-Rutishauser B. Bioavailability of silver nanoparticles and ions: from a chemical and biochemical perspective. J R Soc, Interface. 2013; 10:20130396.

630 Benn T, Westerhoff P. Nanoparticle silver released into water from commercially available sock
631 fabrics. Environ Sci Technol. 2008; 42:4133-4139.

632 Boonkaew B, Kempf M, Kimble R, Cuttle L. Cytotoxicity testing of silver-containing burn
633 treatments using primary and immortal skin cells. Burns. 2014: 40.8: 1562-1569

634 Boukamp P, Petrussevska R, Breitkreutz D, Hornung J, Markham A, Fusenig N. Normal
635 keratinization in a spontaneously immortalized aneuploid human keratinocyte cell line. J Cell
636 Biol. 1988; 106:761-771.

637 Braakhuis HM, Cassee FR, Fokkens PH, de la Fonteyne LJ, Oomen AG, Krystek P, de Jong WH,
638 van Loveren H, Park MV. Identification of the appropriate dose metric for pulmonary
639 inflammation of silver nanoparticles in an inhalation toxicity study. Nanotoxicology. 2016 (in
640 press).Brandenberger C, Mühlfeld C, Ali Z, Lenz A-GG, Schmid O, Parak WJ, Gehr P, Rothen-
641 Rutishauser B. Quantitative evaluation of cellular uptake and trafficking of plain and
642 polyethylene glycol-coated gold nanoparticles. Small. 2010; 6:1669-1678.

643 Brown DM, Dickson C, Duncan P, Al-Attili F, Stone V. Interaction between nanoparticles and
644 cytokine proteins: impact on protein and particle functionality. Nanotechnology. 2010;
645 21:215104.

646 Browning L, Lee K, Nallathamby P, Xu X-HN. Silver nanoparticles incite size- and dose-
647 dependent developmental phenotypes and nanotoxicity in zebrafish embryos. Chem Res
648 Toxicol. 2013; 26:1503-1513.

649 Brunelle JK, Letai A. Control of mitochondrial apoptosis by the Bcl-2 family. J Cell Sci. 2009;
650 122:437-441.

651 Caballero-Díaz E, Pfeiffer C, Kastl L, Gil P, Simonet B, Valcárcel M, Lamana J, Laborda F,
652 Parak WJ. The toxicity of silver nanoparticles depends on their uptake by cells and thus on their
653 surface chemistry. Part Part Syst Char. 2013; 30:1079-1085.

654 Carrola J, Bastos V, Ferreira de Oliveira JM, Oliveira H, Santos C, Gil AM, Duarte IF. Insights
655 into the impact of silver nanoparticles on human keratinocytes metabolism through NMR
656 metabolomics. Arch Biochem Biophys. 2016; 589:53-61.

657 Casals E, Pfaller T, Duschl A, Oostingh GJ, Puntes V. Time evolution of the nanoparticle protein
658 corona. ACS Nano. 2010; 4:3623-3632.

659 Chairuangkitti P, Lawanprasert S, Roytrakul S, Aueviriyavit S, Phummiratch D, Kulthong K,
660 Chanvorachote P, Maniratanachote R. Silver nanoparticles induce toxicity in A549 cells via
661 ROS-dependent and ROS-independent pathways. Toxicol In Vitro. 2013; 27.1: 330-338.

662 Chen X, Schluesener H. Nanosilver: a nanoproduct in medical application. Toxicol Lett. 2008;
663 176:1-12.

664 Comfort KK, Maurer EI, Hussain SM. Slow release of ions from internalized silver nanoparticles
665 modifies the epidermal growth factor signaling response. Colloid Surface B. 2014; 123: 136-
666 142

667 Eckhardt S, Brunetto P, Gagnon J, Priebe M, Giese B, Fromm K. Nanobio silver: its interactions
668 with peptides and bacteria, and its uses in medicine. Chem Rev. 2013; 113:4708-4754.

669 El Badawy AM, Scheckel KG, Suidan M, Tolaymat T. The impact of stabilization mechanism on
670 the aggregation kinetics of silver nanoparticles. Sci Total Environ. 2012; 429:325-331.

671 England C, Priest T, Zhang G, Sun X, Patel D, McNally L, van Berkel V, Gobin A, Frieboes H.
672 Enhanced penetration into 3D cell culture using two and three layered gold nanoparticles. Int J
673 Nanomed. 2013; 8:3603-3617.

674 EPA EPA. State of the Science Literature Review: Everything Nanosilver and More. Scientific,
675 Technical, Research, Engineering and Modeling Support Final Report. 2010.

676 Fernández-López C, Mateo-Mateo C, Alvarez-Puebla R, Pérez-Juste J, Pastoriza-Santos I, Liz-

677 Marzán L. Highly controlled silica coating of PEG-capped metal nanoparticles and preparation
678 of SERS-encoded particles. Langmuir. 2009; 25:13894-13899.

679 Foldbjerg R, Irving E, Hayashi Y, Sutherland D, Thorsen K, Autrup H, Beer C. Global gene
680 expression profiling of human lung epithelial cells after exposure to nanosilver. Toxicol Sci.
681 2012; 130:145-157.

682 George R, Merten S, Wang TT, Kennedy P, Maitz P. In vivo analysis of dermal and systemic
683 absorption of silver nanoparticles through healthy human skin. Australas J Dermatol. 2014;
684 55:185-190.

685 Gliga A, Skoglund S, Odnevall Wallinder I, Fadeel B, Karlsson H. Size-dependent cytotoxicity of
686 silver nanoparticles in human lung cells: the role of cellular uptake, agglomeration and Ag
687 release. Part Fibre Toxicol. 2014; 11.11: 1-17.

688 Greulich C, Diendorf J, Simon T, Eggeler G, Epple M, Köller M. Uptake and intracellular
689 distribution of silver nanoparticles in human mesenchymal stem cells. Acta Biomater.
690 2011;7:347-54.

691 Grosse S, Evje L, Syversen T. Silver nanoparticle-induced cytotoxicity in rat brain endothelial
692 cell culture. Toxicol In Vitro. 2013; 27.1: 305-313.

693 Haberl N, Hirn S, Wenk A, Diendorf J, Epple M, Johnston B, Krombach F, Kreyling W, Schleh
694 C. Cytotoxic and proinflammatory effects of PVP-coated silver nanoparticles after intratracheal
695 instillation in rats. Beilstein J Nanotech. 2013; 4.1: 933-940.

696 Hsiao ILL, Hsieh Y-KK, Wang C-FF, Chen ICC, Huang Y-JJ. Trojan-horse mechanism in the
697 cellular uptake of silver nanoparticles verified by direct intra- and extracellular silver speciation
698 analysis. Environ Sci Technol. 2015; 49:3813-3821.

699 Jeyaraj M, Renganathan A, Sathishkumar G. Biogenic metal nanoformulations induce Bax/Bcl2
700 and caspase mediated mitochondrial dysfunction in human breast cancer cells (MCF 7). RSC
701 Adv. 2015; 5.3:2159-2166.

702 Jiang X, Foldbjerg R, Miclaus T, Wang L, Singh R, Hayashi Y, Sutherland D, Chen C, Autrup H,
703 Beer C. Multi-platform genotoxicity analysis of silver nanoparticles in the model cell line CHO-
704 K1. Toxicol Lett. 2013; 222:55-63.

705 Jokerst JV, Lobovkina T, Zare RN, Gambhir SS. Nanoparticle PEGylation for imaging and
706 therapy. Nanomedicine (Lond). 2011; 6:715-728.

707 Kang S, Lee Y, Lee E-K, Kwak M-K. Silver nanoparticles-mediated G2/M cycle arrest of renal
708 epithelial cells is associated with NRF2-GSH signaling. Toxicol Lett. 2012; 211:334-341.

709 Kennedy AJ, Hull MS, Diamond S, Chappell M, Bednar AJ, Laird JG, Melby NL, Steevens JA.
710 Gaining a critical mass: a dose metric conversion case study using silver nanoparticles. Environ
711 Sci Technol. 2015; 49:12490-12499.

712 Kim S, Choi J, Choi J, Chung K-H, Park K, Yi J, Ryu D-Y. Oxidative stress-dependent toxicity
713 of silver nanoparticles in human hepatoma cells. Toxicol In Vitro. 2009; 23:1076-1084.

714 Kim S, Ryu D-Y. Silver nanoparticle-induced oxidative stress, genotoxicity and apoptosis in
715 cultured cells and animal tissues. J Appl Toxicol. 2013; 33:78-89.

716 Kim TH, Kim M, Park HS, Shin US, Gong MS, Kim HW. Size-dependent cellular toxicity of
717 silver nanoparticles. J Biomed Mater Res Part A. 2012; 100A:1033-1043.

718 Larese FF, D'Agostin F, Crosera M, Adami G, Renzi N, Bovenzi M, Maina G. Human skin
719 penetration of silver nanoparticles through intact and damaged skin. Toxicology. 2009, 255:33-
720 37.

721 Lee Y, Kim D, Oh J, Yoon S, Choi M, Lee S, Kim J, Lee K, Song C-W. Silver nanoparticles
722 induce apoptosis and G2/M arrest via PKCζ-dependent signaling in A549 lung cells. Arch
723 Toxicol. 2011; 85:1529-1540.

724 Li X, Lenhart JJ, Walker HW. Aggregation kinetics and dissolution of coated silver nanoparticles.
725 Langmuir. 2012; 28:1095-1104.

726 Li X, Xu L, Shao A, Wu G, Hanagata N. Cytotoxic and genotoxic effects of silver nanoparticles
727 on primary Syrian hamster embryo (SHE) cells. J Nanosci Nanotechnol. 2013; 13:161-170.

728 Liu W, Wu Y, Wang C, Li H, Wang T, Liao C, Cui L, Zhou Q, Yan B, Jiang G. Impact of silver
729 nanoparticles on human cells: effect of particle size. Nanotoxicology. 2010; 4:319-330.

730 Lu W, Senapati D, Wang S, Tovmachenko O, Singh A, Yu H, Ray P. Effect of Surface Coating
731 on the Toxicity of Silver Nanomaterials on Human Skin Keratinocytes. Chem Phys Lett. 2010;
732 487.

733 Maiorano G, Sabella S, Sorce B, Brunetti V, Malvindi MA, Cingolani R, Pompa PP. Effects of
734 cell culture media on the dynamic formation of protein-nanoparticle complexes and influence on
735 the cellular response. ACS Nano. 2010; 4:7481-7491.

736 Michel R, Pasche S, Textor M, Castner DG. Influence of PEG architecture on protein adsorption
737 and conformation. Langmuir. 2005; 21:12327-12332.

738 Mukherjee SG, O'Claonadh N, Casey A, Chambers G.Comparative in vitro cytotoxicity study of
739 silver nanoparticle on two mammalian cell lines. Toxicol In Vitro. 2012;26:238-51.

740 Nowack B, Bucheli T. Occurrence, behavior and effects of nanoparticles in the environment.
741 Environ Pollut. 2007; 150:5-22.

742 Nowack B, Krug H, Height M. 120 years of nanosilver history: implications for policy makers.
743 Environ Sci Technol. 2011; 45:1177-1183.

744 Nymark P, Catalán J, Suhonen S, Järventaus H, Birkedal R, Clausen P, Jensen K, Vippola M,
745 Savolainen K, Norppa H. Genotoxicity of polyvinylpyrrolidone-coated silver nanoparticles in
746 BEAS 2B cells. Toxicology. 2013; 313:38-48.

747 Oliveira H, Monteiro C, Pinho F, Pinho S, Ferreira de Oliveira JM, Santos C. Cadmium-induced
748 genotoxicity in human osteoblast-like cells. Mutat Res Genet Toxicol Environ Mutagen. 2014;
749 775-776:38-47.

750 Orlowski P, Krzyzowska M, Zdanowski R, Winnicka A, Nowakowska J, Stankiewicz W,
751 Tomaszewska E, Celichowski G, Grobelny J. Assessment of in vitro cellular responses of
752 monocytes and keratinocytes to tannic acid modified silver nanoparticles. Toxicol In Vitro.
753 2013; 27:1798-1808.

754 Park E-JJ, Yi J, Kim Y, Choi K, Park K. Silver nanoparticles induce cytotoxicity by a Trojan-
755 horse type mechanism. Toxicol In Vitro. 2010; 24:872-878.

756 Park J, Lim D-HH, Lim H-JJ, Kwon T, Choi J-sS, Jeong S, Choi I-HH, Cheon J. Size dependent
757 macrophage responses and toxicological effects of Ag nanoparticles. Chem Commun. 2011;
758 47.15: 4382-4384.

759 Pfaffl M. A new mathematical model for relative quantification in real-time RT-PCR. Nucleic
760 Acids Res. 2001; 29.9:e45-e45.

761 Piao MJ, Kang KA, Lee IK, Kim HS, Kim S, Choi JY, Choi J, Hyun JW. Silver nanoparticles
762 induce oxidative cell damage in human liver cells through inhibition of reduced glutathione and
763 induction of mitochondria-involved apoptosis. Toxicol Lett. 2011; 201:92-100.

764 Povoski SP, Davis PD, Colcher D, Martin EW. Single molecular weight discrete PEG
765 compounds: emerging roles in molecular diagnostics, imaging and therapeutics. Expert Rev Mol
766 Diagn. 2013; 13:315-319.

767 Robert, I.M. 2010. Colloidal stability of silver nanoparticles in biologically relevant conditions.
768 Journal of Nanoparticle Research.

769 Rozen S, Skaletsky H. Primer3 on the WWW for general users and for biologist programmers.

770 Methods Mol Biol. 2000; 132:365-386.

771 Sahu SC, Zheng J, Graham L, Chen L, Ihrie J, Yourick JJ, Sprando RL. Comparative cytotoxicity
772 of nanosilver in human liver HepG2 and colon Caco2 cells in culture. J Appl Toxicol. 2014;
773 34:1155-1166.

774 Samberg ME, Oldenburg SJ, Monteiro-Riviere NA. Evaluation of Silver Nanoparticle Toxicity in
775 Skin in Vivo and Keratinocytes in Vitro. Environ Health Perspect. 2010; 118:407-413.

776 Sharma V, Yngard R, Lin Y: Silver nanoparticles: green synthesis and their antimicrobial
777 activities. Adv Colloid Interfac. 2009; 145.1:83-96.

778 Song X-l, Li B, Xu K, Liu J, Ju W, Wang J, Liu X-d, Li J, Qi Y-f. Cytotoxicity of water-soluble
779 mPEG-SH-coated silver nanoparticles in HL-7702 cells. Cell Biol Toxicol. 2012; 28:225-237.

780 Suk JS, Lai SK, Boylan NJ, Dawson MR, Boyle MP, Hanes J. Rapid transport of muco-inert
781 nanoparticles in cystic fibrosis sputum treated with N-acetyl cysteine. Nanomedicine-UK. 2011;
782 6:365-375.

783 Suliman Y AO, Ali D, Alarifi S, Harrath AH, Mansour L, Alwasel SH. Evaluation of cytotoxic,
784 oxidative stress, proinflammatory and genotoxic effect of silver nanoparticles in human lung
785 epithelial cells. Environ Toxicol. 2015; 30:149-160.

786 Suzuki H, Toyooka T, Ibuki Y. Simple and easy method to evaluate uptake potential of
787 nanoparticles in mammalian cells using a flow cytometric light scatter analysis. Environ Sci
788 Technol. 2007; 41: 3018–3024

789 Tao X, Ning Z, Heather LN, Donglu S, Xuejun W. Modification of nanostructured materials for
790 biomedical applications. Mater Sci Eng: C. 2007; 27.3: 579-594.

791 Thorley AJ, Tetley TD. New perspectives in nanomedicine. Pharmacol Therapeut. 2013;
792 140:176-185.

793 Twentyman P, Luscombe M. A study of some variables in a tetrazolium dye (MTT) based assay
794 for cell growth and chemosensitivity. Brit J Cancer. 1987; 56:279-285.

795 Wang X, Ji Z, Chang CH, Zhang H, Wang M, Liao Y-PP, Lin S, Meng H, Li R, Sun B, et al. Use
796 of coated silver nanoparticles to understand the relationship of particle dissolution and
797 bioavailability to cell and lung toxicological potential. Small. 2014, 10:385-398.

798 Wei L, Tang J, Zhang Z, Chen Y, Zhou G, Xi T. Investigation of the cytotoxicity mechanism of
799 silver nanoparticles in vitro. Biomed Mater. 2010; 5:44103.

800 Yang E-JJ, Jang J, Lim D-HH, Choi I-HH. Enzyme-linked immunosorbent assay of IL-8
801 production in response to silver nanoparticles. Methods Mol Biol. 2012; 926:131-139.

802 Zhang T, Wang L, Chen Q, Chen C. Cytotoxic potential of silver nanoparticles. Yonsei Med J.
803 2014; 55:283-291.

804 Zhang W, Yao Y, Sullivan N, Chen Y. Modeling the primary size effects of citrate-coated silver
805 nanoparticles on their ion release kinetics. Environ Sci Technol. 2011; 45:4422-4428.

806 Zhang X-FF, Choi Y-JJ, Han JW, Kim E, Park JH, Gurunathan S, Kim J-HH. Differential
807 nanoreprotoxicity of silver nanoparticles in male somatic cells and spermatogonial stem cells.
808 Int J Nanomed. 2015; 10:1335-1357.

809 Zhao S, Fernald R. Comprehensive algorithm for quantitative real-time polymerase chain
810 reaction. J Comput Biol. 2005; 12:1047-1064.

811 Zucker RM, Daniel KM, Massaro EJ, Karafas SJ, Degn LL, Boyes WK. Detection of silver
812 nanoparticles in cells by flow cytometry using light scatter and far-red fluorescence. Cytometry
813 A. 2013;83(10):962-72.
814

Table 1: Hydrodynamic diameter D_h (with respective polydispersity index PdI) and zeta potential (ζ) of Cit30 and PEG30 AgNPs (30 nm nominal diameter, citrate and polyethyleneglycol coating, respectively) dispersed in ultrapure water or in DMEM culture medium (10 µg/ml). Standard deviations calculated from 3 replicate measurements.

AgNPs		**D_h (nm)**	**PdI**	**ζ (mV)**
Cit30	In water	43.3 ± 0.5	0.25-0.26	-42.7 ± 2.7
	In DMEM	64.8 ± 0.4	0.40-0.41	-8.5 ± 0.4
PEG30	In water	62.1 ± 0.5	0.15-0.16	-12.1 ± 0.5
	In DMEM	57.7± 0.3	0.25-0.27	-6.5 ± 0.4

Figure 1: STEM micrographs of Cit30 and PEG30 AgNPs (30 nm nominal diameter, citrate and polyethyleneglycol coating, respectively) dispersed in deionized water (5 µg/ml).

Figure 2: a) Z-average size and b) % dissolution to Ag+ of Cit30 and PEG30 AgNPs (30 nm nominal diameter, citrate and polyethyleneglycol coating, respectively) incubated in culture medium (10 µg/mL) at 37ºC for 4, 24 and 48h. Error bars correspond to the standard deviations of 3 replicate measurements.

Figure 3: Relative cell viability of HaCaT (%), measured by MTT assay, for 24 h and 48 h. a) Cit30 AgNPs; b) PEG30 AgNPs; c) Citrate – for 24 h and d) PEG – for 24 h. Data expressed as mean and standard deviation. * indicate significant differences between control at $p < 0.05$ for 24h and # indicate significant differences between control at $p < 0.05$ for 48h.

Figure 4: Uptake potential of AgNP by HaCaT cells assessed by the side scattered light by flow cytometry. The results were expressed as the mean +/- SD versus control. ** indicate significant differences between control at $p < 0.01$.

Figure 5: Characterization of intracellular ROS production of HaCaT after exposure to Cit30 and PEG30 AgNPs for 24h, using the DCFDA assay. The results were expressed as the mean +/- SD versus control. ** indicate significant differences between control at $p < 0.01$ and * at $p < 0.05$.

Figure 6: MCP-1 release by HaCaT cells after 24 and 48h exposure to Cit30 and PEG30 AgNPs. Lipopolysaccharide (LPS) was used as a positive control. Data represent the mean ± SEM (n = 3) of the concentration (pg /ml) of MCP-1 cytokine released from the cells after NPs treatment.

Figure 7: Cit30 and PEG30 AgNPs effects on HaCaT cells exposed to 10 and 40µg/mL during 24 and 48h, measured by annexin V assay. Intact cells are represented by "A-P-", dead cells "A-P+", early apoptotic cells "A+P-" and late apoptotic cells "A+P+". Letter A refers to AnnexinV-FITC and letter P refers to propidium iodide. The results were expressed as the mean +/- SD versus control. ** indicate significant differences between control at $p < 0.01$.

Figure 8: HaCaT gene expression of apoptotic genes, after 24h (a) and 48h (b) exposure to Cit30 and PEG30 AgNPs. The results were expressed as the mean relative to control cells (normalized with the GAPDH reference gene) +/- SD versus control.

Figure 9: Effects of AgNPs on cell cycle dynamics, measured by flow cytometry, exposed to Cit30 AgNPs for 24 h a) and 48 h b) and to PEG30coated AgNPs for 24h c) and 48h d). The results were expressed as mean and standard deviation. ** indicate significant differences between control at $p < 0.01$.

Figure 10: HaCaT gene expression of cell cycle genes, after exposure to Cit30 AgNPs for 24 h a) and 48 h b) and to PEG30 AgNPs for 24h c) and 48h d). The results were expressed as mean relative to control cells (normalized with the GAPDH reference gene) and standard deviation. ** indicate significant differences between control at $p < 0.01$.

Figure 11: Principal Component Analysis (PCA) scores scatter plot. The analysis was conducted for the medium values of 48 h AgNPs exposure. “Peg10” and “Peg40” represents PEG- AgNPs 10 µg/mL and PEG- AgNPs 40 µg/mL, respectively; and “Cit10” and “Cit40” represents citrate-AgNPs 10 µg/mL and citrate- AgNPs 40 µg/mL, respectively.

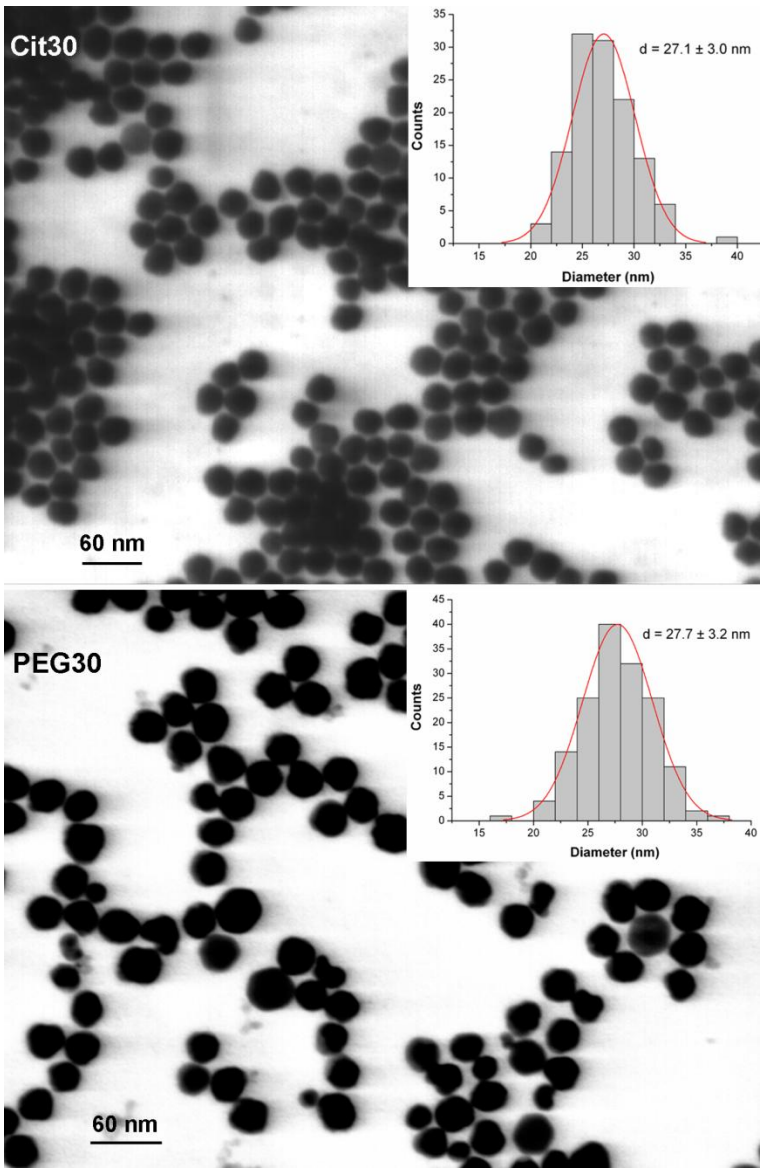

Figure 1

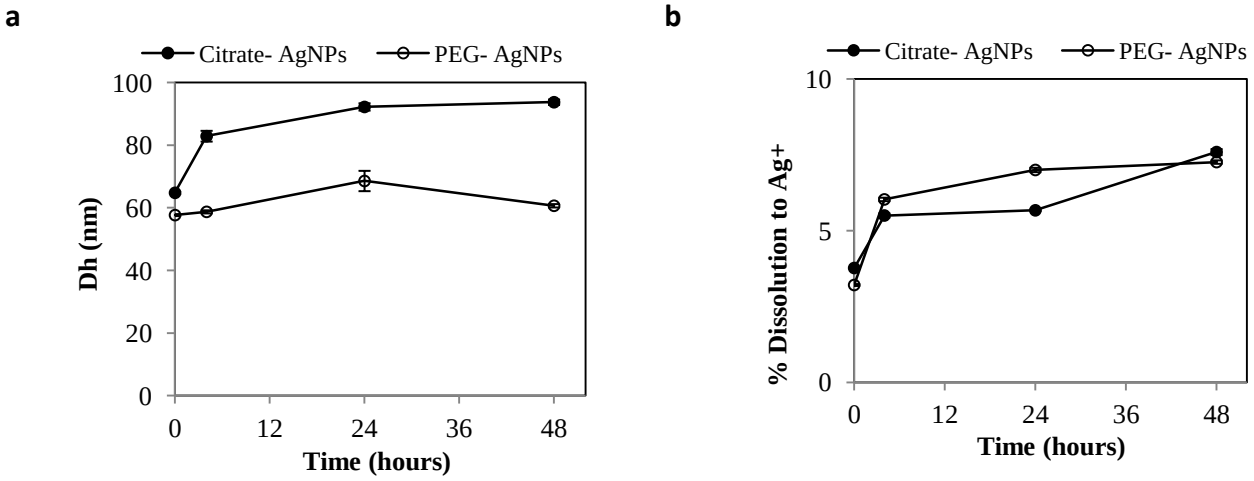

Figure 2

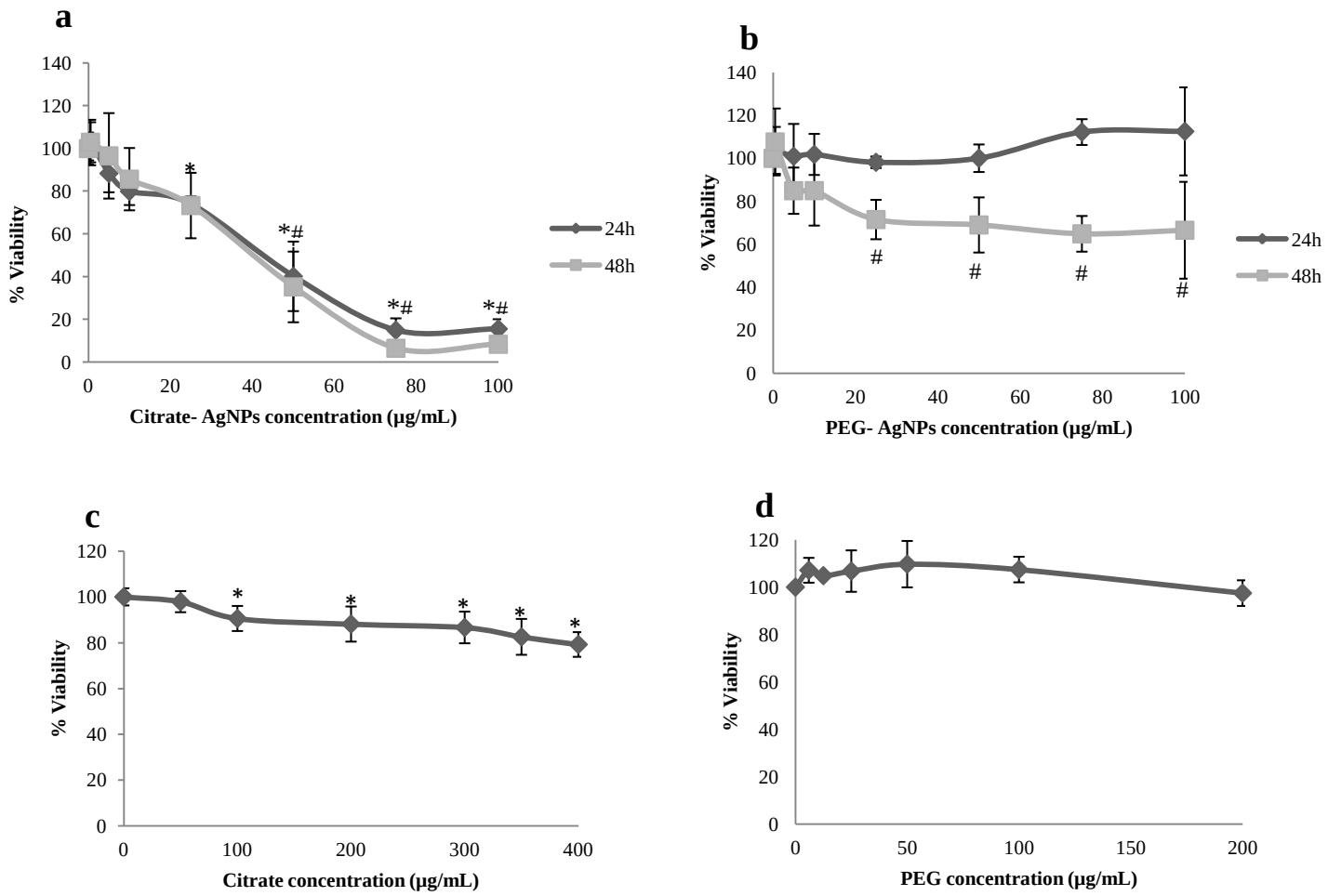

Figure 3

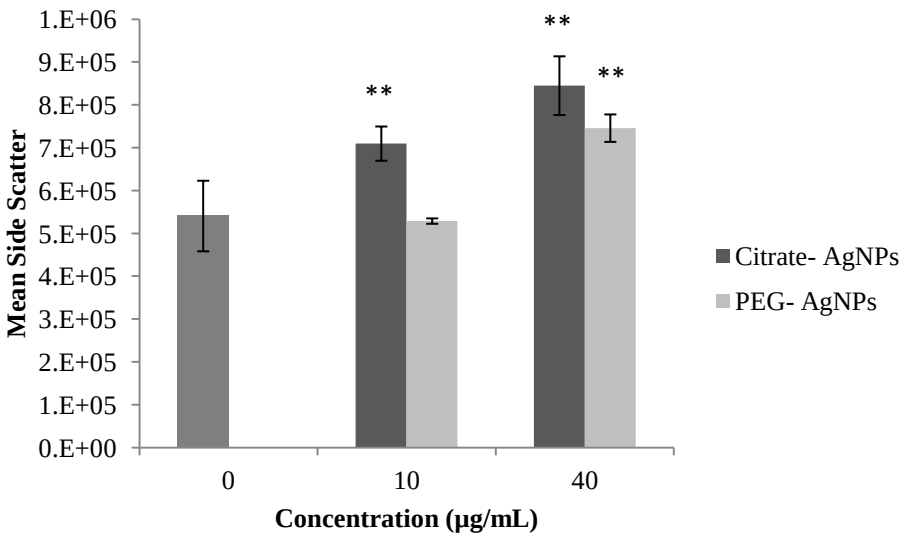

Figure 4

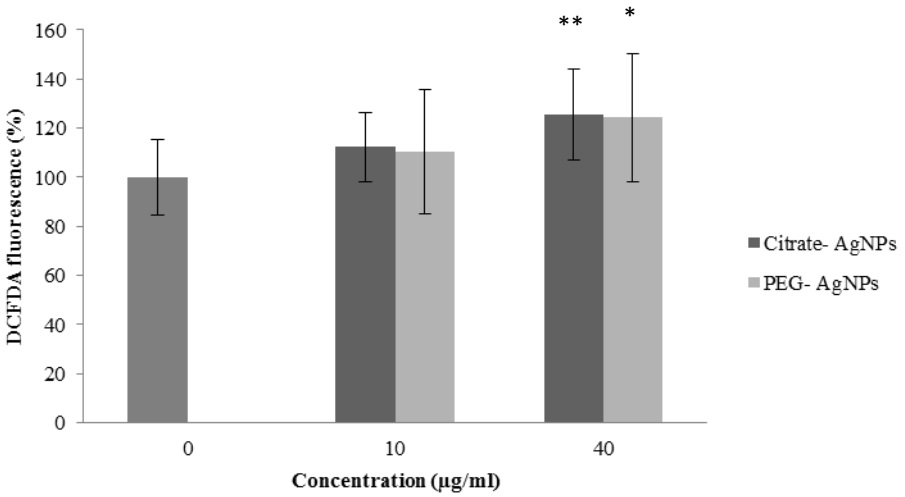

Figure 5

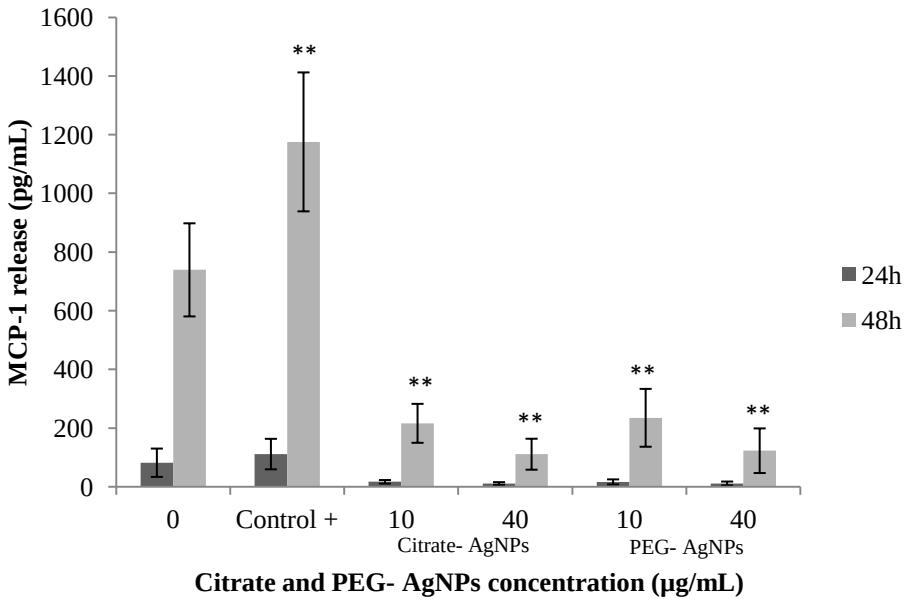

Figure 6

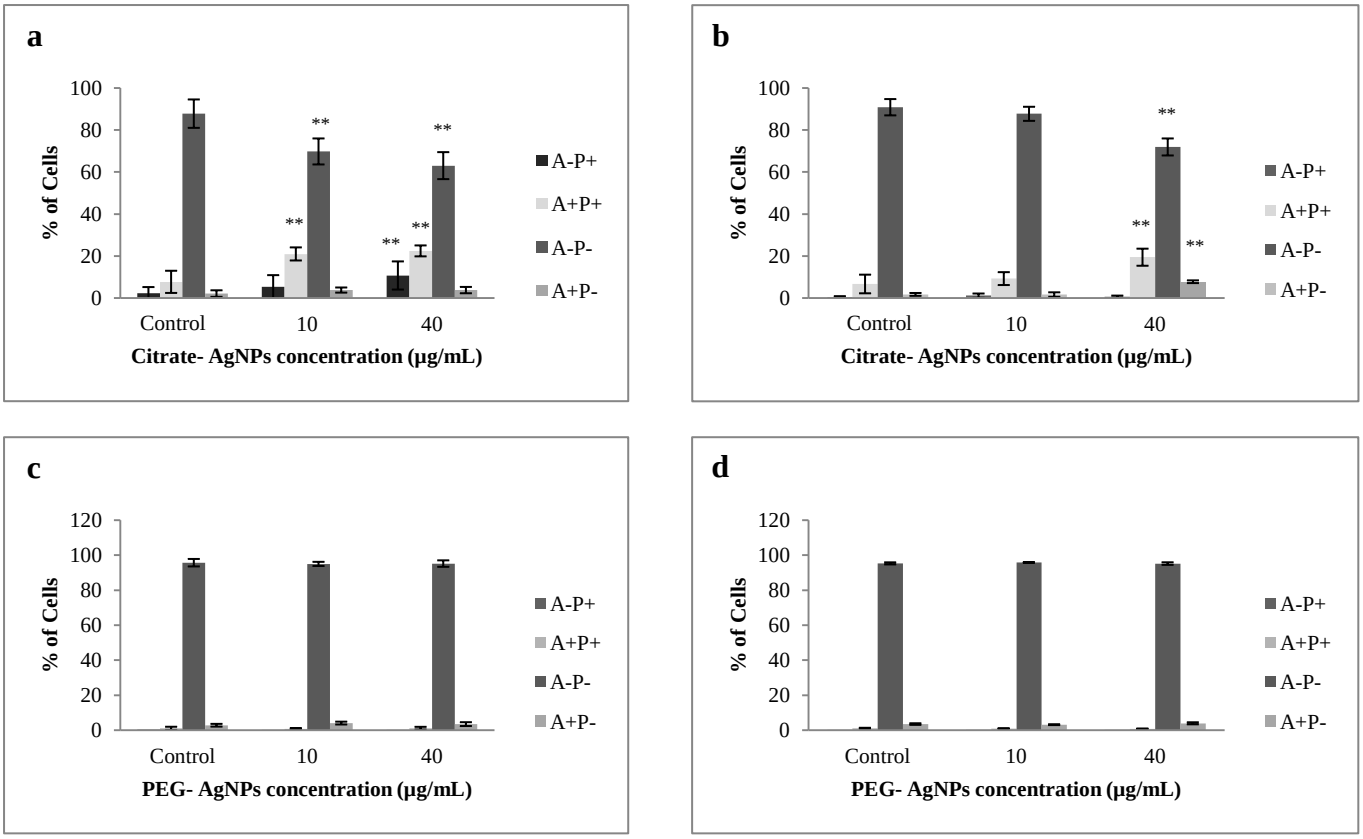

Figure 7

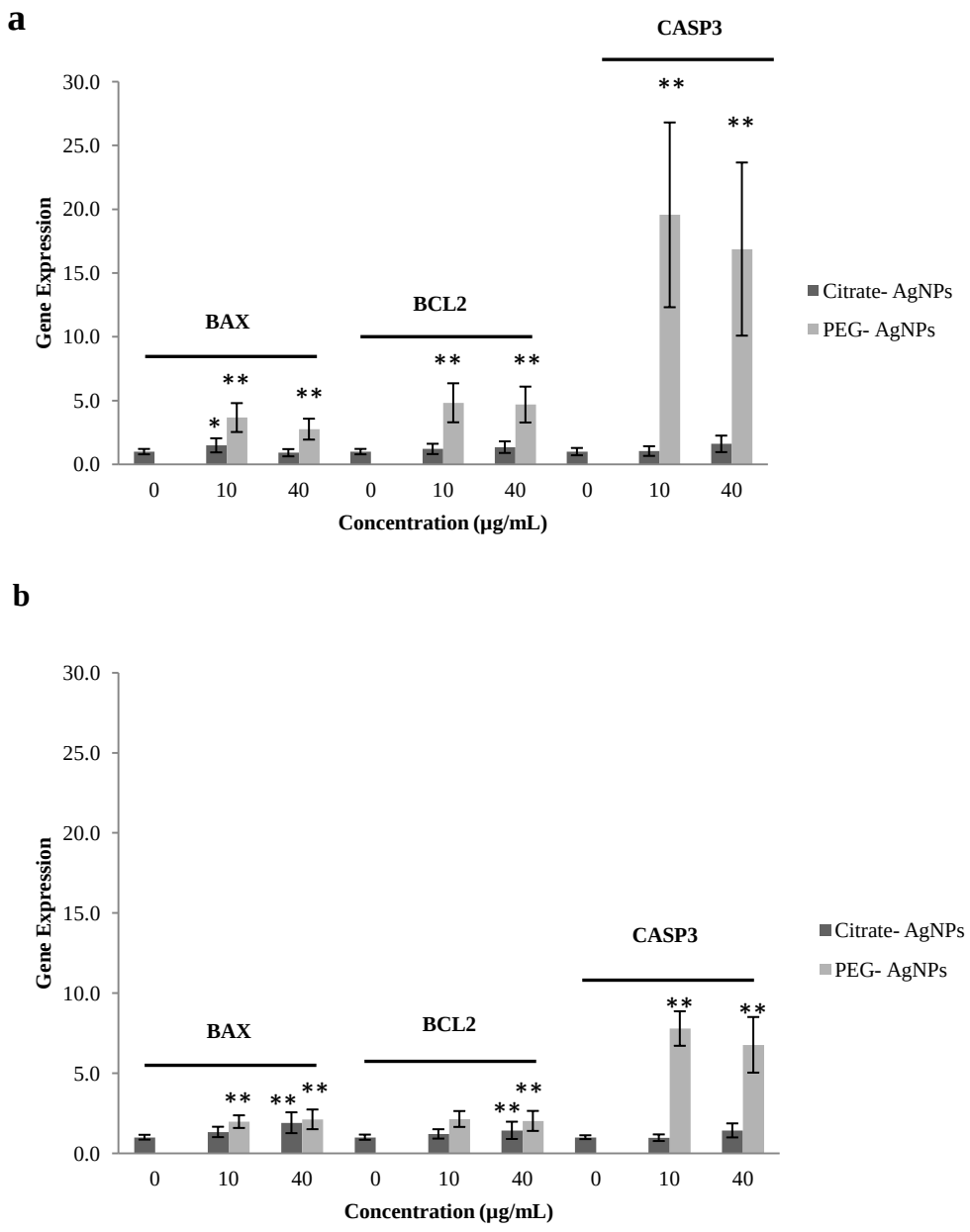

Figure 8

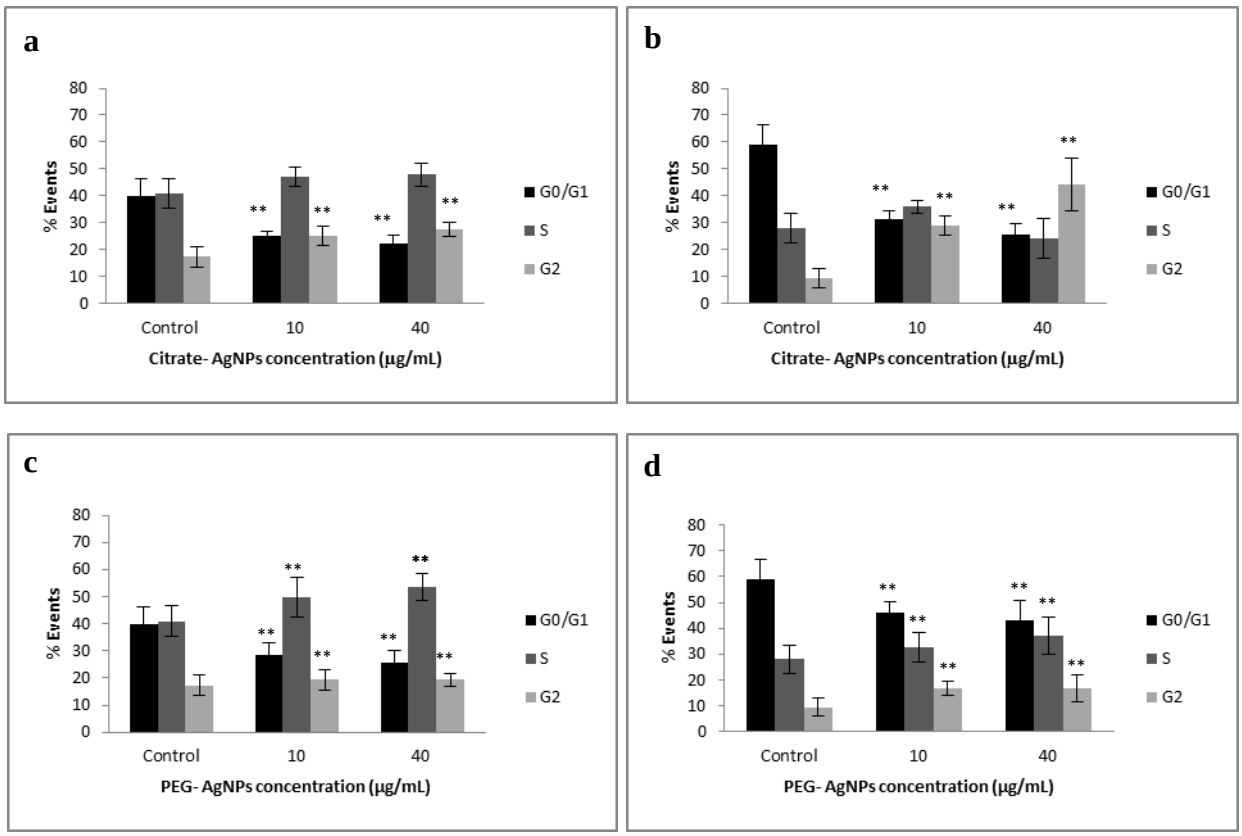

Figure 9

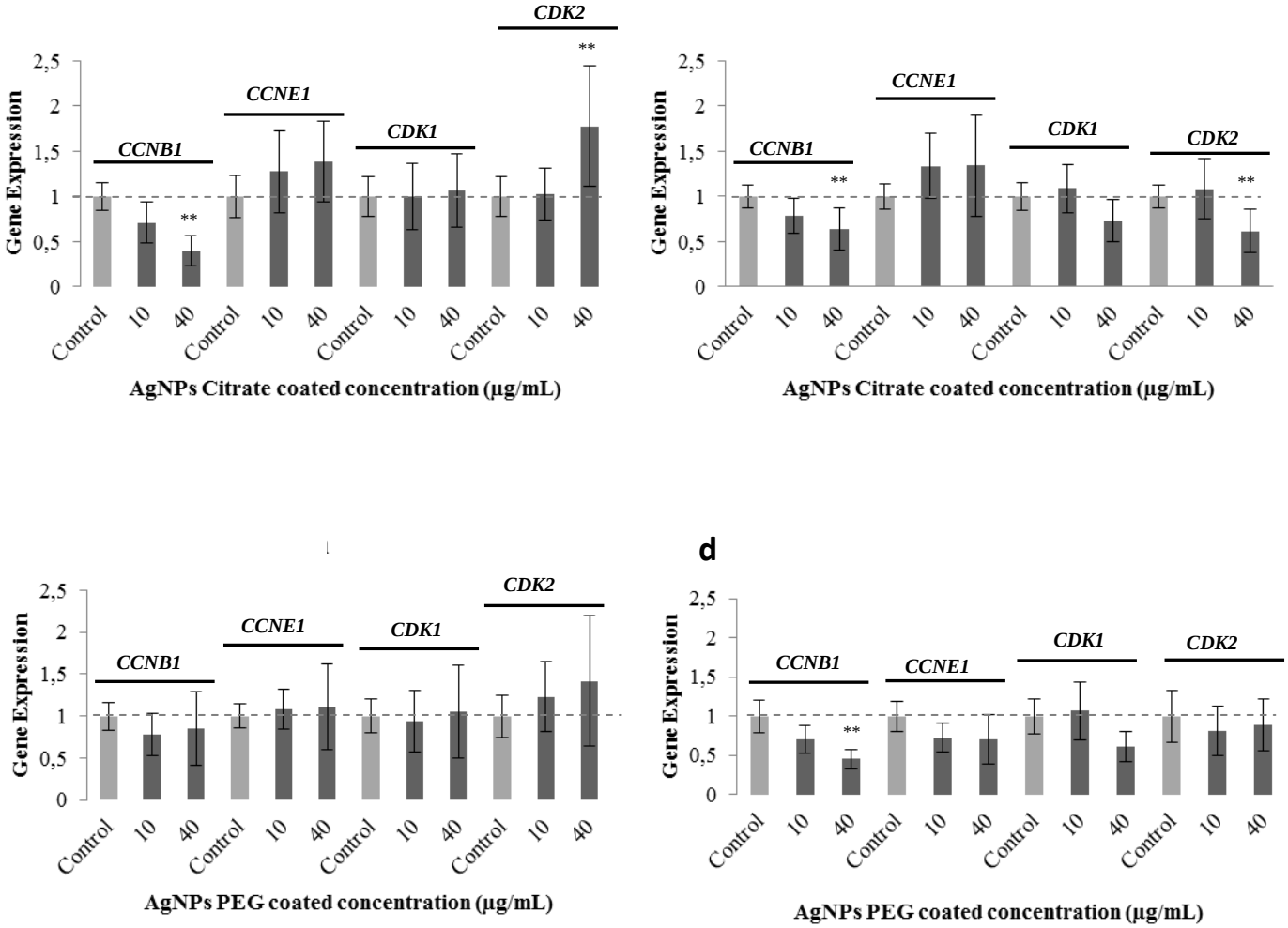

Figure 10

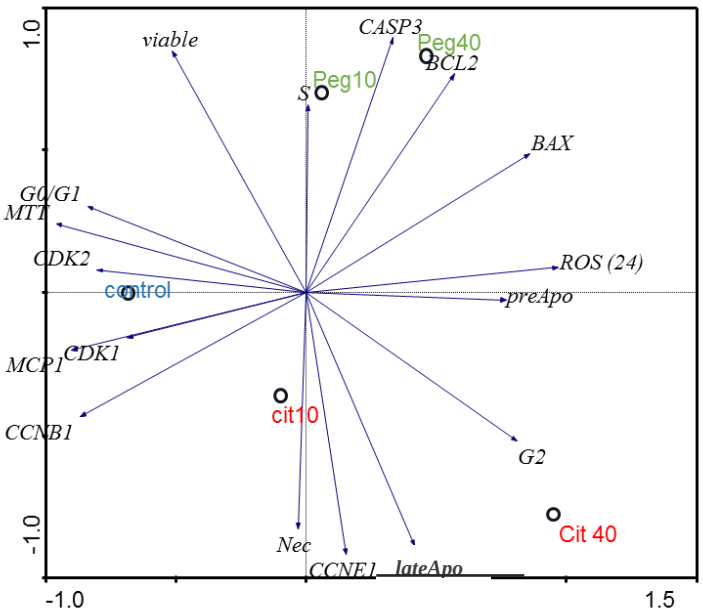

Figure 11